



Article

Laboratory Investigation on Detecting Bridge Scour Using the Indirect Measurement from a Passing Vehicle

Bin Zhang ¹, Hua Zhao ^{1,*}, Chengjun Tan ¹ , Eugene J. OBrien ² , Paul C. Fitzgerald ² and Chul-Woo Kim ³

¹ Key Laboratory for Wind and Bridge Engineering of Hunan Province, College of Civil Engineering, Hunan University, Changsha 410082, China; zb_w1801@hnu.edu.cn (B.Z.); tchj0219@hnu.edu.cn (C.T.)

² Department of Civil Engineering, University College Dublin, D04 V1W8 Dublin, Ireland; eugene.obrien@ucd.ie (E.J.O.); paul.fitzgerald.3@ucdconnect.ie (P.C.F.)

³ Department of Civil and Earth Resources Engineering, Kyoto University, Kyoto 615-8530, Japan; kim.chulwoo.5u@kyoto-u.ac.jp

* Correspondence: zhaohua@hnu.edu.cn

Abstract: For bridges with surface foundations, scour is one of the main reasons for bridge failures. In regard to structural health monitoring, vibration-based scour detection techniques have received increasing attention over the past two decades. Scour occurs below the water surface in rivers or sea, leading to difficulty in equipment installation and maintenance. Recently, the concept of “drive-by” SHM using the indirect measurement of passing vehicle responses has been developed rapidly due to its convenience and low cost. This paper proposes a method to detect scour using the vehicle responses under an operational vehicle speed. The wavelet transform was applied to vehicle accelerations to obtain the wavelet energy. It was found that the wavelet energy increases with the increase in the scour damage level. However, the wavelet energy may also be affected by the on-site operating environments, such as sensor noise and other variabilities, which interferes with the identification of scour in practice. Hence, in this work, a statistical-wavelet-based approach was presented to effectively detect the presence of scour and even its location. The feasibility of the proposed approach is verified in both numerical simulation and lab experiments. The results show that the proposed method has a good potential to detect scour using indirect measurements.

Keywords: bridge scour; indirect measurement; wavelet energy; vibration; SHM; vehicle and bridge interaction



Citation: Zhang, B.; Zhao, H.; Tan, C.; OBrien, E.J.; Fitzgerald, P.C.; Kim, C.-W. Laboratory Investigation on Detecting Bridge Scour Using the Indirect Measurement from a Passing Vehicle. *Remote Sens.* **2022**, *14*, 3106. <https://doi.org/10.3390/rs14133106>

Academic Editor: Giuseppe Casula

Received: 22 May 2022

Accepted: 24 June 2022

Published: 28 June 2022

Publisher's Note: MDPI stays neutral with regard to jurisdictional claims in published maps and institutional affiliations.



Copyright: © 2022 by the authors. Licensee MDPI, Basel, Switzerland. This article is an open access article distributed under the terms and conditions of the Creative Commons Attribution (CC BY) license (<https://creativecommons.org/licenses/by/4.0/>).

1. Introduction

Wardhana and Hadipriono [1] studied more than 500 bridge failures in the US from 1989 to 2000 and pointed out that the most common cause of bridge failure was attributed to scour. Scour is the engineering term for the soil erosion surrounding a bridge foundation [2]. Scour erosion causes a local reduction in soil elevation around the foundation, resulting in reduced foundation stiffness, which affects the carrying capacity of the bridge foundation system [3]. Bridge failures caused by scouring are characterized as sudden and catastrophic. As one of the unprevented natural hazards, major floods often yield peaks in the frequency of bridge failures [4]. In addition, the destroyed bridges in flooding result in traffic interruption and thus block the delivery of relief supplies. It is noted that with the increasing number of bridges across rivers or seas, the issue of bridge scour has become increasingly prominent [5]. Therefore, how to maintain the safe operation of bridges under scouring has become an urgent problem to be solved. Since foundation scour occurs below the water surface, the bridge scour is concealed, and it is difficult to detect and diagnose directly. Traditionally, diving inspection is adopted, but it has some disadvantages, namely that it is labor-intensive, subjective, and dangerous to undertake during flooding [6]. In addition, vision-based diving inspections are challenged because scour holes tend to refill with sediment after floodwaters recede [4].

With the development of sensor technology, bridge inspection research based on the concept of structural health monitoring (SHM) has increasingly attracted attention. In general, there are two methods for scouring detection using SHM: direct measurements and indirect measurements. Methods based on the direct measurements use the bridge responses, e.g., accelerations, displacements, and strains to detect scour [7–14]. Bridge scour causes changes in foundation stiffness, which result in changes in bridge boundaries [15]. Therefore, for direct measurements, the changes in frequencies are often extracted to assess the bridge scour conditions. For example, Prendergast, Hester, Gavin, and O’Sullivan [9] experimentally showed that when a single pile of a bridge is affected by scour, the natural frequency of the bridge changes significantly. In addition, they proposed a method for estimating the scour depth based on a given observed pile frequency. However, indicators based on frequency variation cannot directly reflect the scour location of bridges with multiple foundations. Furthermore, the natural frequency of bridges is also affected by temperature variations [16], which may interfere with the determination of scour.

In order to address it, as a relatively recent development, the extracted modal shape was represented as a scouring indicator [17,18]. Scozzese et al. [19] numerically demonstrated that Operational Modal Analysis could be used to monitor scour in masonry multi-arch bridges and even reflect the extent of the damage. In order to detect scour locations, two modes are usually compared at different health states of the bridge [20]. Technically, the modal shape-based methods imply that a large number of sensors need to be installed on the bridge structure [15]. In order to reduce the number of sensors, some signal processing-based mode shape extraction methods were proposed, e.g., multi-setup and decentralized techniques [21,22]. However, these methods obviously reduce the resolution of extracted modal shapes or increase the amount of repetitive work.

Compared to direct measurement, indirect measurement means that there are no sensors installed on the bridge. The analyzed signals are from a moving vehicle as it passes over the bridge, which is referred to as a “drive-by” bridge monitoring system [23]. Yang et al. [24] first proposed the concept of “drive-by” bridge SHM and verified its feasibility by extracting the natural frequencies of the bridge from the accelerations of passing vehicles. The theoretical background of “drive-by” is that when a vehicle travels over the bridge, the induced vehicle responses under the vehicle–bridge interaction contain information about the dynamic parameters of the bridge. Regarding bridge SHM, the indirect measurements show many advantages in terms of economy, mobility, equipment necessity, specialist personnel on-site, simplicity, and efficiency [25].

With a bridge–vehicle–wave interaction model, Kong and Cai [26] numerically studied the effect of scour on bridge responses and vehicle responses. They noted that both responses of bridge decks and passing vehicles were able to detect the presence of scour by finding the change in the extracted natural frequency of the bridge. This suggests that the “drive-by” bridge SHM is also one of the potentially effective methods to detect scour. Fitzgerald et al. [27] numerically investigated the feasibility of using train accelerations to detect scour damage in railway bridges. They proposed a damage indicator based on the difference in wavelet coefficients of train accelerations between the scour and non-scoured bridge conditions.

In bridge SHM, wavelet transform, as a robust signal processing tool, is frequently used to detect damage and even damage location [23,27–32]. For example, Chatterjee et al. [33] applied continuous wavelet transform (CWT) on responses of an instrumented bridge to improve the axle identification of a moving vehicle in the bridge weigh-in-motion system. Hester and Gonzalez [34] applied CWT on the acceleration of a traveling vehicle to detect the bridge crack and its location. It was also found that the indirect measurement, i.e., vehicle acceleration is more effective than the direct measurement, i.e., bridge acceleration, at detecting small cracks. For scour detection, O’Brien et al. [35] developed a method to detect scour location using wavelet-based Operating Deflection Shape (ODS) amplitudes. Direct measurements, i.e., bridge acceleration measurements at each support location, were used to generate the damage indicator based on the ODS differences between non-scoured

and scoured conditions. The feasibility of the proposed method was numerically verified by a bridge model with four simply supported spans resting on piers. As previously described, Fitzgerald, Malekjafarian, Cantero, O'Brien, and Prendergast [27] proposed a wavelet-based approach to detect scour on railway bridges through indirect measurements. The validity of this method is also only verified by numerical models.

Drive-by/indirect measurement bridge SHM has potential applications in detecting scour, which has the advantage of low cost and convenience. Since the “drive-by” bridge SHM is a relatively recent development, the study on the application of scouring detection using indirect measurements is very limited so far. This paper proposes a drive-by scour detection method based on wavelet transform. A lab experiment was carried out to verify the proposed method in addition to numerical models. In this paper, the feasibility of indirect measurement in scours detection was first verified by laboratory experiments. Furthermore, the sensitivity of the sensor location was investigated in laboratory experiments.

Most bridge SHM applications with CWT use its characteristic of signal discontinuity. In contrast, this paper applied the CWT to vehicle accelerations to measure the wavelet energy at a scale/pseudo frequency, which is related to the bridge's natural frequency. It was found that the measured energy increased when the bridge scour occurred. In numerical simulations, sensor noise and environmental variables were considered in this work. The environmental variables were introduced by setting different road profiles in the vehicle–bridge interaction model. Due to the influence of the on-site operating environment, a few test results have certain variability and cannot correctly reflect the real situation of bridge scour. Therefore, this paper proposes a statistical-based method to detect the presence of scour. In addition, because wavelet energy has no localization information, this paper also proposes an index to locate the scour pier using the component wavelet energy. Both numerical simulation and lab experiments showed that the proposed method has a good potential to detect scour with indirect measurements.

2. Numerical Modelling

Erosion of the soil under and around the bridge foundation can reduce its stiffness. Therefore, a simple bridge model with reduced foundation stiffness was used to simulate bridge scour caused by soil erosion. Figure 1 shows the numerical model of the vehicle–bridge interaction (VBI) system. This bridge scour model has been adopted in many studies [3,4,15,27,35,36].

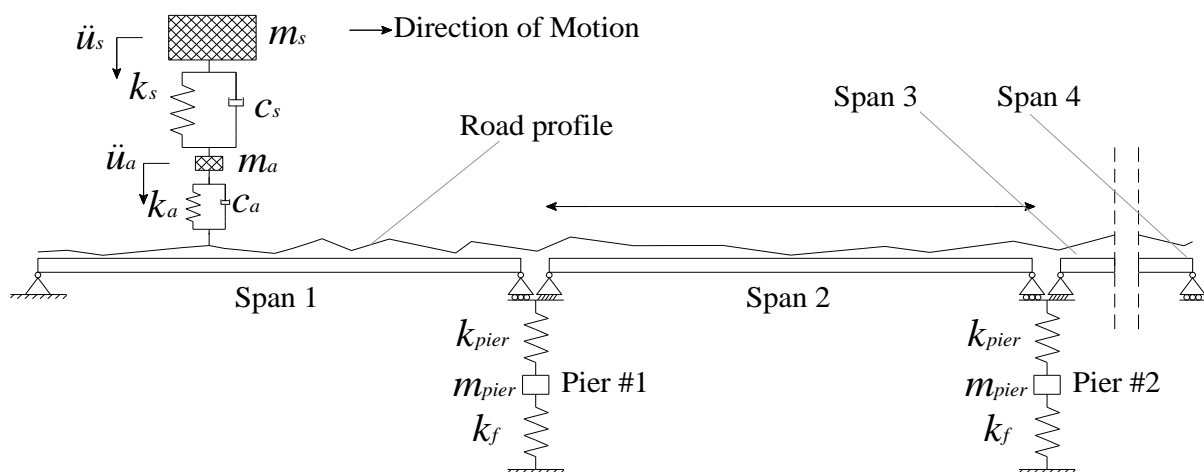


Figure 1. The VBI system.

2.1. Vehicle Model

A quarter-car model with 2 degrees of freedom (DOF) was adopted in this study. The vehicle masses were modeled with a sprung mass m_s , and un-sprung mass m_a , which are represented by the vehicle body mass and wheel mass, respectively. Their bouncing

degrees of freedom are labeled as u_s and u_a , respectively. The wheel stiffness and damping are represented by k_a and c_a , respectively. The vehicle suspension stiffness and damping are represented by k_s , and c_s , respectively. The dynamic equation of the vehicle is described by Equation (1).

$$[M_v]\{\ddot{y}_v\} + [C_v]\{\dot{y}_v\} + [K_v]\{y_v\} = \{f_v\}, \quad (1)$$

where K_v , C_v , and M_v are represented by the matrix of the vehicle stiffness, damping, and mass, respectively; y_v denotes the vertical displacement of the vehicle, including the translations of body mass (u_s) and wheel (u_a). The external force vector f_v is a function of the bridge displacements and the road profile. The properties of the vehicle model in this study are listed in Table 1, based upon the work of [37,38]. Under these parameters, the two frequencies of the vehicle are 0.57 Hz and 9.89 Hz.

Table 1. Properties of the quarter-car model.

Vehicle Parameters	Symbol	Unit	Value
Body mass	m_s	kg	14,300
Wheel mass	m_a	kg	700
Suspension stiffness	k_s	kN/m	200
Suspension damping	c_s	kN s/m	100
Wheel stiffness	k_a	kN/m	2500
Wheel damping	c_a	kN s/m	10

2.2. Bridge Model

As shown in Figure 1, a four-spans single-lane bridge was modeled. Each span was simulated as a 1D finite element, consisting of 20 Euler–Bernoulli beam elements. Both ends of the bridge rest on non-deformable supports modeled as pins and rollers. Adjacent spans are connected with hinged supports, which rest on deformable piers, modeled as a single DOF sprung mass in the vertical direction. m_{pier} and k_{pier} represent the pier mass and stiffness, respectively. It is noted that each pier is modeled with the same parameters. Each pier rests on a shallow pad foundation, which is represented by a spring with a stiffness of k_f . The length, L , and width, B , of the shallow pad foundation, are assumed of 4 and 2 m, respectively. Based on these pad dimensions, k_f can be determined using the approach in FEMA [39] as follows:

$$k_f = \frac{GB}{1-\nu} \left[1.55 \left(\frac{L}{B} \right)^{0.75} + 0.8 \right], \quad (2)$$

where G represents the operational shear modulus of the soil; ν represents the small-strain Poisson ratio. The soil shear modulus G is calculated using the expression $G = E/(1 + \nu)/2$, where $E = 100,000$ kPa [9]. Note that Equation (2) is a semi-empirical calculation, and there are some similar expressions available in Refs. [40,41]. The properties of the bridge system are listed in Table 2. In this paper, a reduction in stiffness of the vertical foundation spring, k_f , was used to model bridge scour. The damage level was defined as the reduction percentage of k_f . More detail of the bridge scour model is given in Refs. [3,15,27].

Table 2. Properties of bridge model [15].

Bridge Property	Symbol	Unit	Value
Span length	L	m	20
Beam depth	D	m	1
Beam second moment of area	I_b	m ⁴	0.33
Beam mass per unit length	m_b	kg·m ⁻¹	9.6×10^3
Beam modulus of elasticity	E_b	kN·m ⁻²	35×10^6
Pier mass	m_{pier}	kg	42×10^3
Pier stiffness	k_{pier}	kN·m ⁻¹	12.5×10^6
Stiffness provided by foundation	k_f	kN·m ⁻¹	344.12×10^6

An approach with 50 m was adopted to ensure the equilibrium of vehicle dynamic behavior before it enters the bridge. In this study, the road surface profile with “class A” was randomly generated according to the power spectral density curve, as described in ISO 8608 [42]. The bridge dynamic equation due to the time-varying forces was modeled as:

$$[M_b]\{\ddot{y}_b\} + [C_b]\{\dot{y}_b\} + [K_b]\{y_b\} = [L]\{f_b\}, \quad (3)$$

where M_b , C_b , and K_b are the mass, damping, and stiffness matrixes of the bridge system (including beams and foundations), respectively, and y_b represents the bridge displacement. \dot{y}_b and \ddot{y}_b denote the first and second derivatives of y_b , respectively, with respect to time, which represent the bridge’s vertical velocity and acceleration responses, respectively. Damping is considered in the bridge system using the Rayleigh type with a damping ratio of 3%. The vector f_b is the time-varying interaction forces between the vehicle and the bridge in a VBI system. Those interaction forces were distributed to the relevant DOFs of beams utilizing a location matrix L , which took into account the wheel location at each moment. Vehicle–bridge interaction is a coupled system and can be represented by Equation (4).

$$\begin{bmatrix} M_v & 0 \\ 0 & M_b \end{bmatrix} \begin{Bmatrix} \ddot{y}_v \\ \ddot{y}_b \end{Bmatrix} + \begin{bmatrix} C_v & C_{v,b} \\ C_{b,v} & C_b \end{bmatrix} \begin{Bmatrix} \dot{y}_v \\ \dot{y}_b \end{Bmatrix} + \begin{bmatrix} K_v & K_{v,b} \\ K_{b,v} & K_b \end{bmatrix} \begin{Bmatrix} y_v \\ y_b \end{Bmatrix} = \{F\}, \quad (4)$$

where F is the force vector applied to the coupled system. The method of the Wilson–Theta integration was used to solve the coupled system [43]. The MATLAB programming environment was applied to mimic the numerical vehicle–bridge interaction and post-processing.

3. Scour Detection Approach

3.1. Wavelet Analysis

Wavelet analysis is a robust signal processing technique that has been widely used in SHM [31]. Mathematically, the wavelet transform is similar to the Fourier transform in that a given signal or function $f(t)$ is approximated using a family of functions constructed from a single function (mother wavelet) by dilation and translation. Unlike the Fourier transform, which only performs as a signal-converting tool from the time domain to the frequency domain, the wavelet transform exhibits outstanding localization properties in both the time and frequency domains. Equation (5) provides the mathematical definition of the wavelet transform.

$$WT(a, b) = \int_{-\infty}^{+\infty} f(t) \frac{1}{\sqrt{a}} \Psi_{a,b}(t) dt, \quad (5)$$

where $WT(a, b)$ is the wavelet transforms and $\Psi_{a,b}(t)$ is given as follows:

$$\Psi_{a,b}(t) = \frac{1}{\sqrt{a}} \Psi\left(\frac{t-b}{a}\right), \quad (6)$$

$\Psi_{a,b}(t)$ is called the daughter wavelet derived from the mother wavelet $\Psi(t)$, which satisfies the properties of $\int_{-\infty}^{+\infty} \Psi(t) dt = 0$ and $\int_{-\infty}^{+\infty} |\Psi(t) dt| < \infty$; a and b denote the parameters of the scale and translation, respectively.

When CWT is applied to a signal, it produces a series of wavelet coefficients at each scale in the time domain. The scale is related to signal frequency. For a small value of scale, a , the corresponding wavelet coefficients are implied to have a high-frequency content. While for a large value of scale, a , it means that the given signal is approximated using a stretched wavelet function, so the wavelet coefficients have low-frequency components. In mathematics, the relationship between scale and wavelet frequency is defined as follows:

$$F_s = \frac{F_c}{a\Delta}, \quad (7)$$

where F_s is called wavelet pseudo-frequency, a is the scale of wavelet transforms, Δ is the sampling period of the signal, and F_c is the central frequency of the mother wavelet.

Energy is one of the unique measurements of a given signal. The energy of the wavelet coefficients at scale a and location b is expressed by:

$$E(a, b) = |WT(a, b)|^2, \quad (8)$$

Then the total energy of the function at a particular scale, a , is expressed as:

$$E_{tol}(a, b) = \sum_{b=1}^N |WT(a, b)|^2, \quad (9)$$

where N is the total number of wavelet coefficients. Gao and Yan [44] pointed out that for a given signal, if there are dominant frequency components, the energy of its wavelet coefficients shows higher magnitudes at the corresponding scales. Thus, the energy plot can reflect the dominating frequencies in the signal.

Figure 2a shows the vehicle acceleration response at a speed of 14 m/s (around 50 km/h) using the VBI model described above. The vehicle response was applied to CWT using the wavelet function of “db2”, and the percentage of energy at each scale is illustrated in Figure 2b. The wavelet function of “db2” was chosen because it was verified to be effective in bridge SHM [45]. Unless otherwise mentioned, CWT adopts the wavelet function of “db2” in this paper. As shown, the dominant frequency components appear near the 1st natural frequency of the bridge. First, it demonstrates the feasibility of the concept of “drive-by” SHM since the passing vehicle contains information on bridge parameters. Second, the identified frequency is not exact with the bridge frequency, but this phenomenon is consistent with the findings of Cantero et al. [46]. They presented that the different suspension properties with the same vehicle mass cause different frequency shifts in the natural frequencies of the bridge.

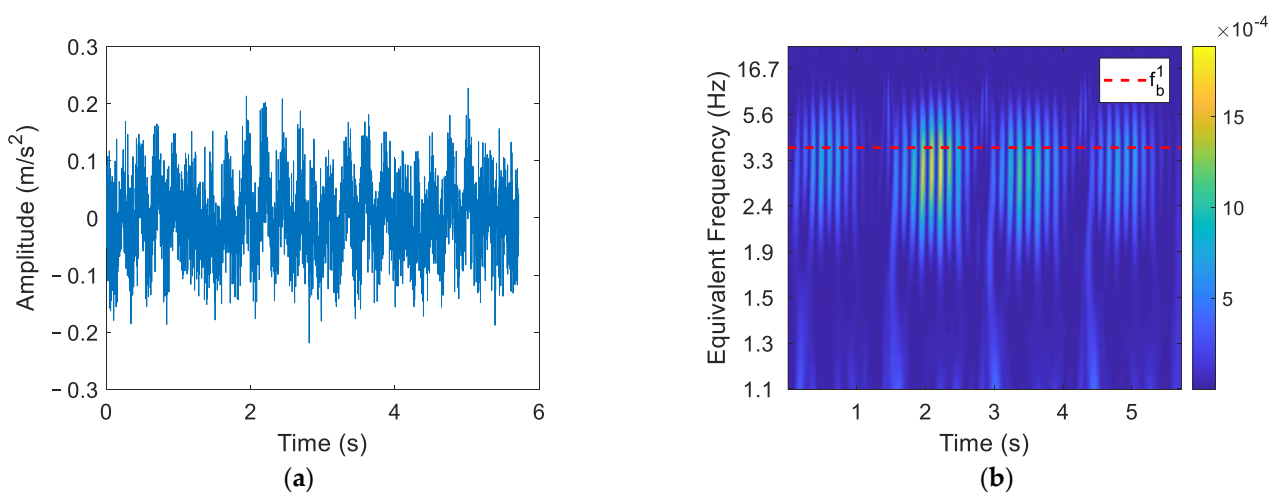


Figure 2. Vehicle response and wavelet energy; (a) vehicle acceleration; (b) percentage of energy at different frequencies (scales) (Note: f_b^1 represents the bridge’s 1st natural frequency).

Figure 3 shows a comparison of the total energy plots at two different conditions of the bridge. The solid line represents the case in Figure 2, i.e., no damage, while the stippled line represents the situation where the bridge scours at Pier 3 with a damage level of 25%. In this comparison, all others were kept the same except for bridge conditions. As shown, the change in the first natural frequency of the bridge is weak and imperceptible, but the wavelet energy peak significantly increases as scour damage occurs. This may be because the reduction in the stiffness of the foundation amplifies the vibration of the moving vehicle so as to increase the wavelet energy of the vehicle acceleration. The results reflect that the change in bridge frequencies is not a robust indicator for scouring detection in this model.

Wavelet-based energy is more reliable as a damage indicator for detecting bridge scour. It is numerically demonstrated that the proposed wavelet-based method has the potential to detect scour damage using indirect measurements.

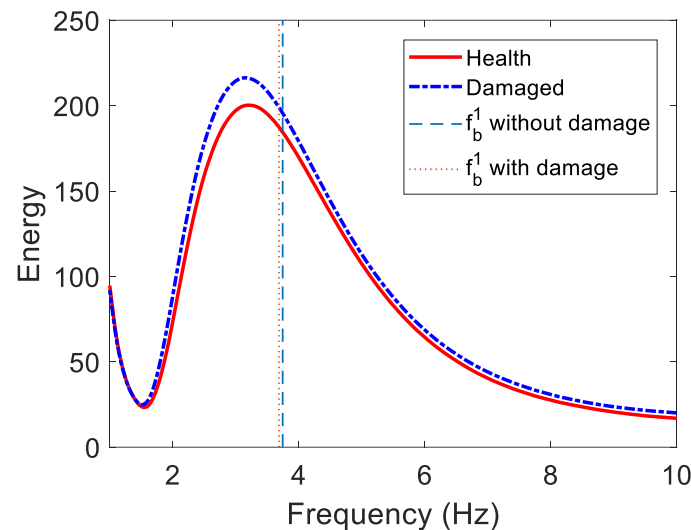


Figure 3. Comparison of wavelet total energy at different frequencies (scales).

3.2. Addition of Environment Variable to Vehicle Acceleration

In order to detect bridge scour, the proposed method requires baselines in health conditions for comparison. In practice, the environment may be different for each vehicle traveling, including sensor noise. This difference may also cause a change in the total energy of the wavelet, which interferes with the identification of bridge scour. In order to investigate it, sensor noise was considered in this study. The random noise was added to the vehicle acceleration using Equation (10) [46].

$$\{S\} = \{S_{calc}\} + E_p \{N_{noise}\} \sigma, \quad (10)$$

where S is the polluted response to the vehicle acceleration, E_p represents the level of the noisy signal, N_{noise} represents a standard normally distributed vector with a unit standard deviation, S_{calc} represents the generated clean response of acceleration, and σ is its standard deviation. In this study, the noisy level, E_p , was arbitrarily chosen to be 5%, which is consistent with that in Refs. [27,47,48]. In addition, to further mimic the difference in the environment, in the VBI model, a “class A” road roughness was also randomly generated for each run. In other words, in the simulation, each run has a different road profile, but all at the “class A” level.

3.3. A Statistical-Wavelet-Based Scour Detection Method

In this section, five bridge scour conditions were simulated in the VBI model. The scour was located at Pier 3, and the damage levels are 0%, 15%, 25%, 35%, and 45%, respectively. For each scenario, 50 runs were simulated at the same vehicle speed of 14 m/s. As aforementioned, the sensor noise and road surface profile were randomly generated on each run. Figure 4 illustrates all those wavelet energies for 250 runs with a boxplot. In this boxplot, it gives information about the median, minimum, maximum, first quartile, third quartile, and individual outlying points underlying statistical distribution. As shown in Figure 4, some wavelet energies at different scour levels overlap each other due to different environments, especially at lower scour levels. Thus, it is not feasible to achieve high-accuracy scour detection by testing a few times.

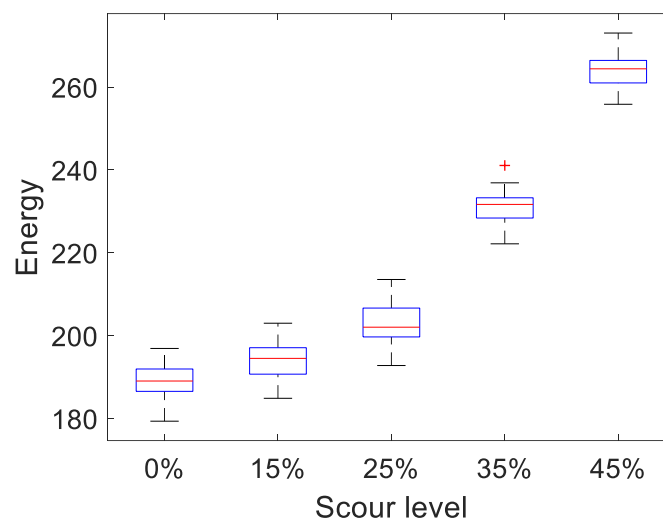


Figure 4. Energy distribution on different scour levels.

Therefore, this paper proposed a method based on statistical wavelet energy to detect bridge scour. A batch of runs was used to characterize bridge scour conditions. First, a normal probability distribution was fitted on the first batch, with the mean value of μ and the standard deviation value of σ . This probability distribution represents a baseline for the bridge condition. For bridge scour monitoring, a new run substituted the oldest run of that batch, and the normal probability distribution was updated, with the mean value of μ_1 and the standard deviation value of σ_1 . Although the parameters of the distribution are updated, two distributions may share a large number of areas. Many damage detection approaches use $\mu \pm \sigma$ to solve the problem of shared areas [49]. The confidence interval of $\mu \pm \sigma$ has a confidence level of almost 70%. This paper also used a confidence level of around 70% to represent the bridge condition. Considering the fact that the wavelet energy increases rather than decreases due to bridge scour, $\mu + \sigma/2$ was used to quantify the baseline bridge condition because the confidence interval of $[-\infty \quad \mu + \sigma/2]$ has a confidence level of almost 70%. Similarly, the reference line was represented as $\mu_1 - \sigma_1/2$ in the updated distribution, because the confidence interval of $[\mu - \sigma/2 \quad +\infty]$ was also with a confidence level of almost 70%. In other words, this paper determined the presence of scour occurrence when the value of $\mu_1 - 0.5\sigma_1$ was more than the values of $\mu + 0.5\sigma$.

3.4. Detecting Scour Location

In order to detect scour locations, this study proposed a pier index using the component energy associated with each span. For the sake of clarity, it was assumed here that the scour is identified at the distribution, where the mean value is μ_d and the standard deviation value is σ_d . The previous distribution (corresponding to a health condition) has the mean value and standard deviation value of μ_h and σ_h , respectively. Those distribution parameters were obtained from the whole vehicle acceleration responses, S , when the vehicle travels across the entire bridge. In this study, the bridge had four spans. Thus, the entire acceleration, S , could be equally divided into four parts, and each part represents the responses when the vehicle passes over the corresponding span, labeled as S_i ($i = 1, 2, 3$, and 4 , represents the span No.). For a batch of S_i , a normal probability distribution can also be fitted on them. For the health condition, the mean and standard deviation values of the distributions were labeled as μ_h^i and σ_h^i , respectively. For the scoured condition, those values were labeled as μ_d^i and σ_d^i , respectively. The pier index is then defined as Equation (11).

$$ID_{pier}^i = \Delta_{i+1} - \Delta_i \quad (i = 1, 2, \text{ and } 3), \quad (11)$$

where

$$\Delta_i = (\mu_d^i - \mu_h^i) / (\mu_d - \mu_h) \quad (i = 1, 2, 3, \text{ and } 4), \quad (12)$$

Theoretically, when scour occurs on Pier i , all wavelet energy components change to some extent due to the integrity of the bridge structure. This study found that $\Delta_{j \leq i}$ did not change much in most cases, but $\Delta_{j > i}$ increased significantly to some extent. Therefore, scour occurs on the Pier i , resulting in a maximum value of ID_{pier}^i among $ID_{pier}^{1 \sim 3}$. The effectiveness of the proposed pier index was verified by both numerical analysis and lab experiments as follows. Thus far, this paper proposed a statistical wavelet-based method that utilizes vehicle responses to detect bridge scour and even uses component wavelet energy to identify scour locations. In practice, once a bridge scour is detected during the monitoring process, manual inspections can be triggered to obtain more damage detail and identify the source of damage. The flowchart of bridge scour detection with indirect measurements is expressed as shown in Figure 5.

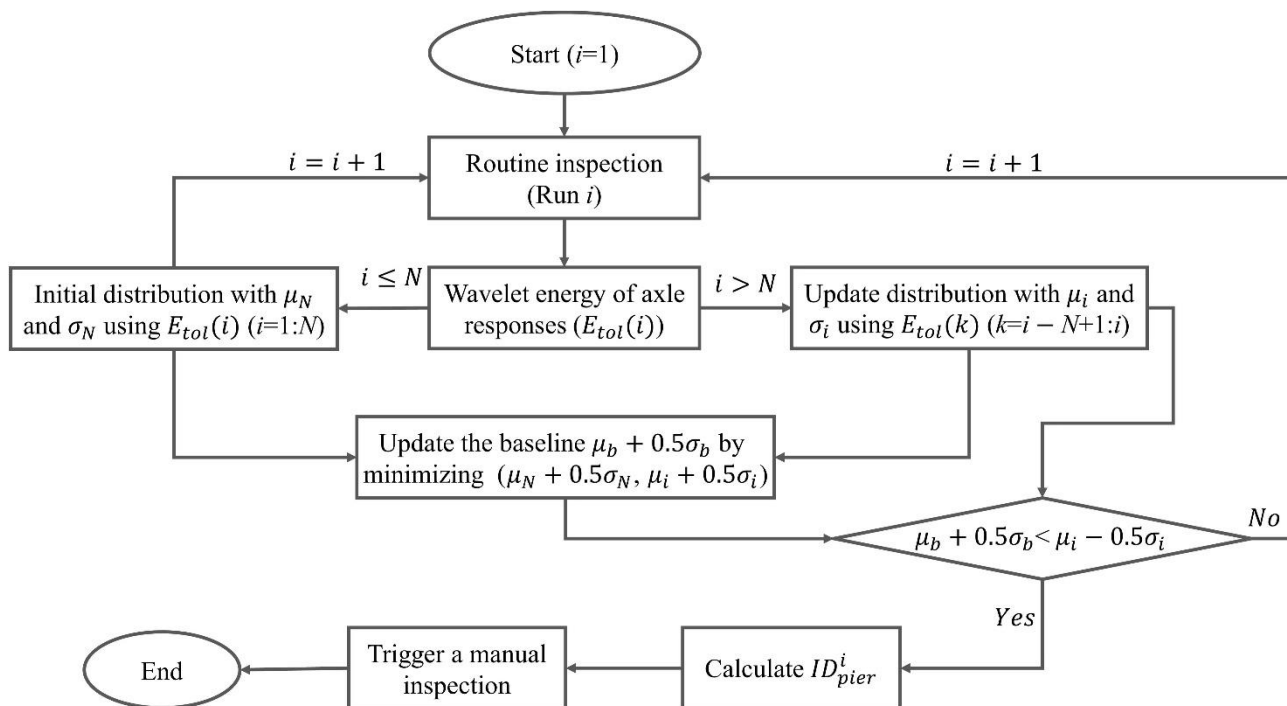


Figure 5. Flowchart of scour detection (note: N represents the number of distribution samples).

4. Numerical Verification

4.1. Scour Detection on Different Piers

In order to verify the feasibility of the proposed approach, the case with five bridge conditions in Figure 4 was studied. First, for each bridge condition, a normal probability distribution was fitted on the batch of those 50 runs. Figure 6a shows the fitted distribution under the non-scoured condition. Admittedly, it did not quite fit the normal distribution, but that is not surprising given the small sample size. All fitted distributions for five bridge conditions are plotted in Figure 6b. As shown, there are apparent shifts for those fitted distributions due to scours. In addition, as the scour level increases, the shift distance also increases. Figure 6c illustrates the range of mean value \pm standard deviation/2 for each fitted distribution. Compared to the non-scoured condition, each level of bridge scour can be detected because all the reference lines for the scoured distributions (mean value $-$ standard deviation/2) are greater than the baseline (mean value $+$ standard deviation/2) for the non-scoured condition. Moreover, the reference lines for all higher scour damage levels are also larger than the corresponding baselines for lower scour levels, reflecting the feasibility of detecting scour levels. It notes that, in this case, the degree of shift in the fitted distribution approximates a parabolic growth as the level of bridge scour increases.

In order to identify the scour location, the proposed pier indexes were calculated based on Equation (11), and the results are plotted in Figure 6d. It should be noted that, in

this case, scour occurs on Pier 3. As shown in Figure 6d, except for the scour level of 15%, the pier index ID_{pier}^3 is the highest value among $ID_{pier}^{1\sim3}$. The result indicates that the pier index can successfully detect the scour location if the scour level is greater than 15%. This pier index fails at the scour level of 15% because the proposed approach is not sensitive to the lower level of scour damage at Pier 3, as shown in Figure 6c.

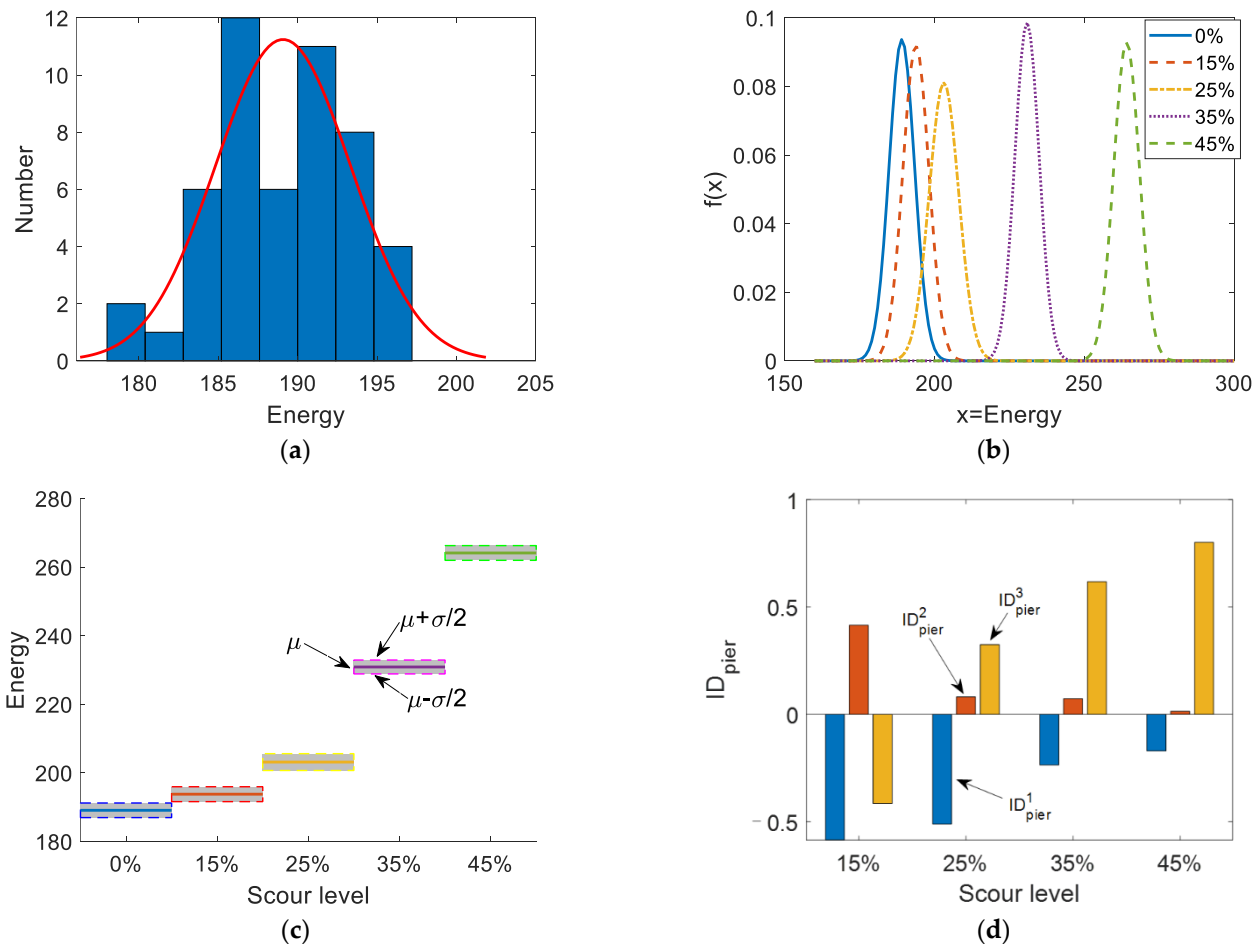


Figure 6. Results of scour detection on Pier 3; (a) a normal probability distribution fitted on 50 runs without scour; (b) probability distributions for different scour levels; (c) ranges of $\mu \pm 0.5\sigma$ for each distribution; (d) pier index, ID_{pier}^i , $i = 1, 2, 3$.

In the following study, bridge scour was set at Pier 2 in the VBI model. All others were consistent with previous studies. The scour detection results are illustrated in Figure 7. As shown, in this case, bridge scour can be clearly detected using the proposed approach (Figure 7a). For the Pier 3 bridge scour, the growth rate of the shift extent increases with an increase in the scour level. In contrast, this growth rate decreases for the Pier 2 bridge scour. Figure 7b shows the identification of the bridge scour location. As expected, ID_{pier}^2 has maximum value among $ID_{pier}^{1\sim3}$ for all scour levels. The results validate the effectiveness of the proposed pier index for detecting bridge scour locations. Unlike scour that occurs on Pier 3, the pier index is also effective even at a low scour level on Pier 2. This is because the proposed method is sensitive to detecting bridge scour that occurs at Pier 2.

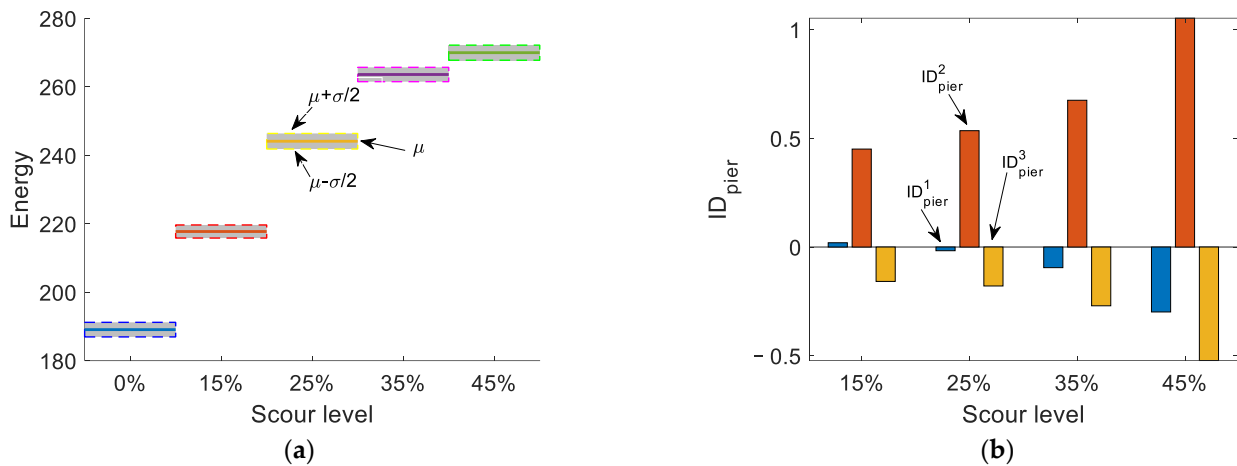


Figure 7. Scour detection on Pier 2; (a) ranges of $\mu \pm 0.5\sigma$ for each distribution on different scour levels; (b) the scour location indicator on piers, ID_{pier}^i , $i = 1, 2, 3$.

In order to describe the accuracy of the detection, the probability of detection (POD) method is usually used in non-destructive testing [50]. A POD curve can show the detection probability for tested results. In this paper, the reference indicator was wavelet energy. Therefore, a POD curve versus energy was approximated using a Logit function, defined as in Equation (13) [51].

$$POD(E_{tol}) = \frac{e^{\frac{\ln(E_{tol}) - \mu}{\sigma}}}{1 + e^{\frac{\ln(E_{tol}) - \mu}{\sigma}}}, \quad (13)$$

where μ and σ are constant parameters that define the curve. All previous simulated data were used to determine these two parameters. In these data, when the bridge scour occurs, the probability of detection is 1, whereas that is 0 for non-scour conditions. These data were plotted in Figure 8, as well as the fitted curve. This curve can be used to qualify the reliability of the inspection system for the following bridge scour identification.

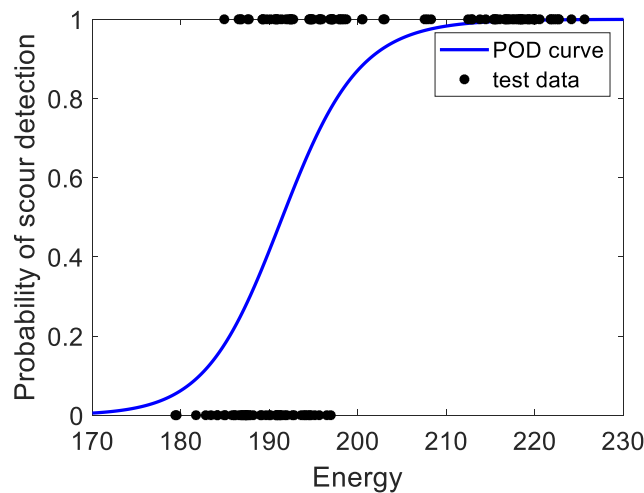


Figure 8. The fitted POD curve.

4.2. Blind Simulation Tests

In this section, a test with continuous measurements is simulated to simulate the real-world situation of scour detection using a passing vehicle. A total of 1400 runs were generated using the described VBI model. Environment variables were also considered for each run. In this test, each run was represented here as an event. These 1400 events were measured in consecutive order. The bridge was first modeled under the non-scoured

condition. Bridge scour was then introduced into the VBI model at some point in time. This moment was randomly generated among 1400 events. Hence, every event that occurred before this moment had a non-scoured bridge, and every event after this moment had a scoured pier. The scoured pier and its damage level were also randomly generated. In other words, in regard to those 1400 events, the user was only given 1400 responses of vehicle accelerations without information on the scoured moment, the scoured location, and the scoured severity. In the following, the proposed approach, as shown in Figure 5, was used to detect bridge scour with a batch of 200 events. It should be noted that the actual scour happens after the first 200 events.

First, a normal distribution was fitted on accelerations of the first 200 events, and the mean value and standard deviation were labeled as μ_{200} and σ_{200} , respectively. Second, the event of 201 substitutes the first event to update the parameters on a normal distribution, and they were labeled as μ_{201} and σ_{201} , respectively. Then the event of 202 was used to replace the second event, and so on. As already mentioned, if the value of $\mu_{m+1} - \sigma_{m+1}/2$ ($m > 200$) is greater than the minimum value of $\mu_n + \sigma_n/2$ ($n = 200 \sim m$), the scour was detected, and it can trigger a manual inspection in the real world. If not, the test considers this event as “normal” and proceeds to the next test. In this case, the results are shown in Figure 9a. The scour was detected at event 946 because $\mu_{946} - \sigma_{946}/2$ is greater than the value of $\mu_{200} + \sigma_{200}/2$, where $\mu_{200} + \sigma_{200}/2$ is the minimum value of $\mu_k + \sigma_k/2$ ($k = 200 \sim 945$). It was noted that the actual scour occurs at event 893.

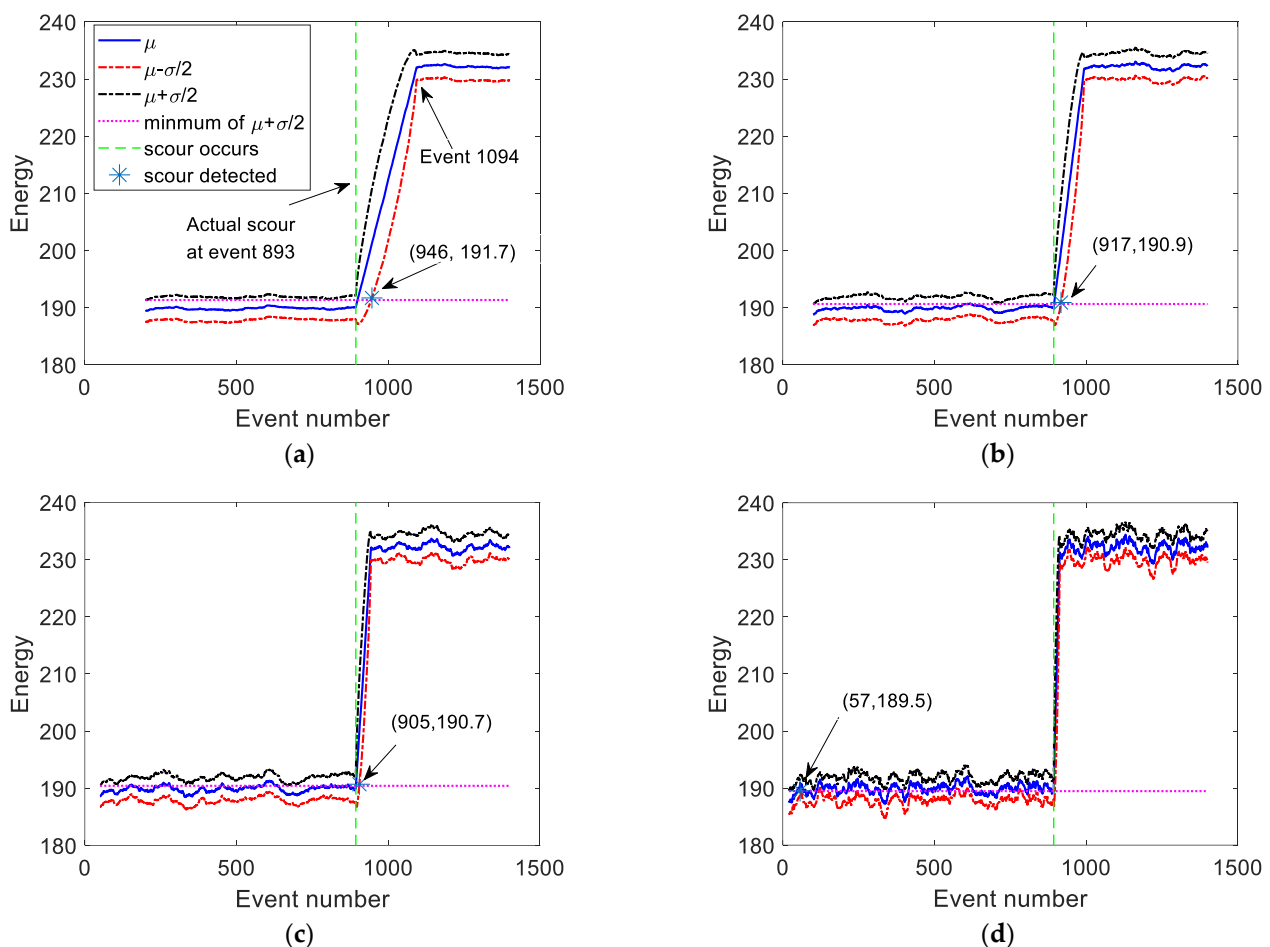


Figure 9. Scour detection in blind tests; (a) batches of 200 runs; (b) batches of 100 runs; (c) batches of 50 runs; (d) batches of 20 runs.

As shown in Figure 9a, the range of $\mu_{m+1} \pm \sigma_{m+1}/2$ varies smoothly before the scour event and gradually increases after the bridge scour. Bridge scour cannot be detected

immediately using the proposed method because each distribution is updated with only one new event. The value of $\mu_{m+1} \pm \sigma_{m+1}/2$ gradually increases as the number of runs under scour conditions increases so that scour can be detected. In effect, the value of $\mu_{m+1} \pm \sigma_{m+1}/2$ still increases after bridge scour detection until all runs of the distribution are under scour conditions. That is to say, the range of $\mu_{m+1} \pm \sigma_{m+1}/2$ stops increasing clearly around the event 1093 ($=893 + 200$). It is well understood that the jump in the values of $\mu_{m+1} \pm \sigma_{m+1}/2$ is a clearer indicator for bridge scour detection. However, more events after bridge scours are required, indicating that detection is not timely. Once the scour occurs, it would be risky to conduct extensive driving tests on this bridge. The sooner it is detected, the better for traffic control and bridge maintenance. The proposed method can successfully detect the bridge scour after only about 50 runs using a batch of 200.

Similarly, batch runs of 100, 50, and 20 were applied to detect the presence of bridge scour. The results are shown in Figure 9b–d, respectively. As shown, all of them also present a clear jump after the scour event. In addition, the magnitude of change in the plots of μ_{m+1} and $\mu_{m+1} \pm \sigma_{m+1}/2$ increases with decreasing run batches. Both batches of 100 and 50 can successfully detect the presence of bridge scour in time, with recognitions at events of 917 and 905, respectively. However, the proposed approach with batches of 20 fails in bridge scour detection due to the high-intensity vibrations of the distribution parameters. It concludes that the less batch of runs can detect scour faster but has a greater chance of making wrong decisions. It is suggested that the batch runs should not be less than 50.

In this blind simulation, the scour location was also unknown. For those three successful detection cases (batch runs of 200, 100, and 50), their corresponding pier indexes are calculated based on Equation (11) in order to detect the scour location. It should be noted that in this equation, μ_d uses the distribution parameters at the detected event while μ_n uses the baseline values that have the minimum value of $\mu_n + \sigma_n/2$ in the detection. The results are illustrated in Figure 10. For all cases, ID_{pier}^2 has the maximum value indicating that scour is clearly identified to happen at Pier 2, which is consistent with the fact. Blind tests further demonstrate the feasibility and effectiveness of the proposed approach in detecting the presence of scour and identifying the scoured pier. In fact, the blind simulation depicts how the proposed approach was implemented in the real world. The specific instrumented vehicle owned by the bridge manager travels across the objective bridge with a routine inspection. For each run, the measurement data were first used to check whether safety limits were exceeded. If so, the possible scour piers were calculated, and manual inspections could be triggered for more scour details. If not, it was used to update the distribution parameters.

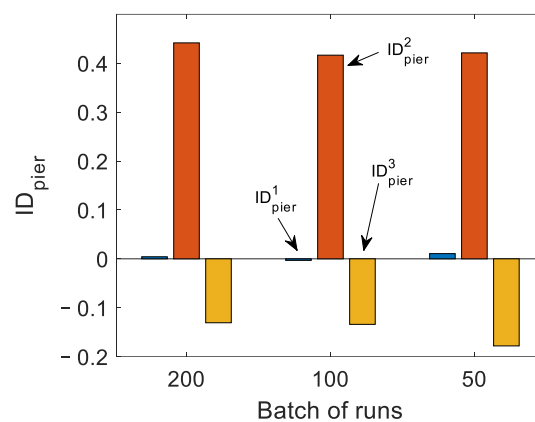


Figure 10. Detecting scour location in blind tests.

In addition, the previously fitted POD curve can be used to examine the reliability of this bridge scour inspection. In general, for a POD method, an important indicator is “90/95”, where “90” denotes the detection probability of 90%, with a confidence level of

95%. For this blind test, Figure 11 illustrates the confidence level for scour detection at a 90% probability of each run. As shown, before the scour event, this confidence level was very low (varies around 0.2). Therefore, these results are untrusted. In contrast, after the scour event, most of the confidence levels were as high as over 95%, and this result means that we found the bridge scour with a 90% chance, and we are over 95% sure about it.

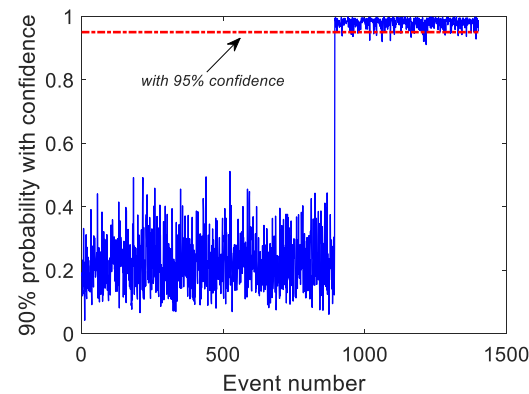


Figure 11. The confidence at a 90% detection probability.

5. Lab Experiment Validation

In order to further verify the feasibility of the proposed approach, a laboratory experiment was carried out at the University of Kyoto, as shown in Figure 12. In this laboratory test, a scaled bridge was constructed, which has four simply supported spans. Both two ends of the bridge have rigid support, and the three internal piers are supported on springs to represent the vertical stiffness provided by pad foundations. Extra lengths were given to allow the traveling vehicle to accelerate and decelerate. Table 3 lists the properties of each span. By using the FDD (frequency domain decomposition) algorithm [7], the first three natural frequencies of the bridge were identified as 9.77 Hz, 11.72 Hz, and 14.06 Hz, respectively [36].

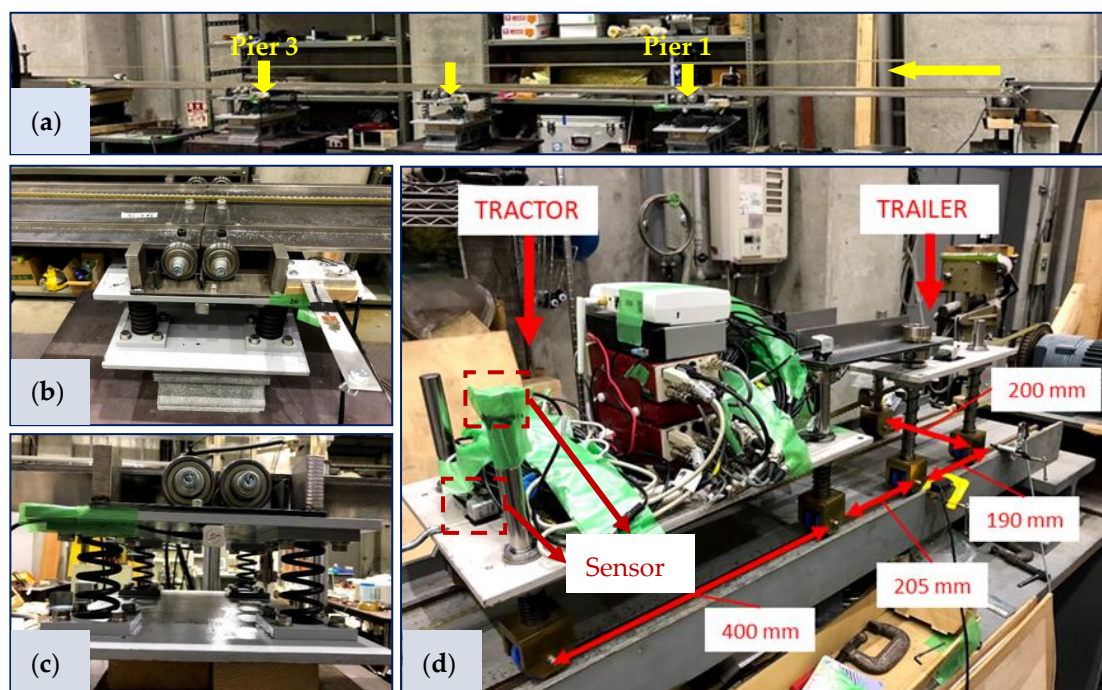


Figure 12. Experimental test: (a) a scaled bridge model; (b) bridge supports; (c) pier detail; (d) vehicle model and sensor locations.

Table 3. The properties of each span.

Property	Unit	Value
Span length	m	1.3
Span width	mm	300
Span depth	mm	8.07
Second moment of area (Rectangular cross section)	m ⁴	1.314×10^{-8}
Young's Modulus	N m ⁻²	2.05×10^{11}
Density	kg m ⁻³	7850

As shown in Figure 12c, each pier was represented by four support springs. The combined stiffness of each pier was calculated as 196 N mm^{-1} ($=4 \times 49 \text{ N mm}^{-1}$) based on a load–displacement test. This experiment used a static scaling criterion to choose the value of the support stiffness appropriately. Thus, the reference indicator is the ratio of bridge mid-span deflection (for a unit load applied on mid-span) to foundation deflection (for a unit load directly applied above the support). This ratio is kept the same between a full-scale benchmark case and the experimental case. The method of Adhikary et al. [52] was used to calculate the foundation stiffness for the full-scale benchmark, where the pad foundation was assumed to have dimensions of $2 \text{ m} \times 4 \text{ m}$. In order to simulate foundation scour, the support springs were replaced with lesser stiffness ones. Two cases were considered. For case I, each spring with 37 N mm^{-1} was used to support piers, whereas a spring with 27 N mm^{-1} was used for case II. Thus, two bridge scour levels (24.5% and 44.9%) were simulated in this experiment compared to the non-scoured condition, and the scour was located at either Pier 2 or Pier 3, as shown in Figure 12a.

Figure 12d shows the experimental vehicle with a tractor-trailer system. Both the tractor and trailer have four sprung wheels with a steel plate resting on these springs. The stiffnesses of the front and rear axle of the tractor are 3066 N m^{-1} (i.e., $2 \times 1533 \text{ N m}^{-1}$ springs) and 3506 N m^{-1} (i.e., $2 \times 1753 \text{ N m}^{-1}$ springs), respectively. The trailer has an equal stiffness of $16,928 \text{ N m}^{-1}$ on each axle (i.e., $2 \times 8464 \text{ N m}^{-1}$). The tractor and trailer have total masses of 24.3 kg and 13.7 kg, respectively. By using FDD, the pitch and bounce frequencies of the tractor were extracted as 4.7 Hz and 3.1 Hz, respectively, and those for the trailer are 3.5 Hz and 6.6 Hz, respectively. Two acceleration sensors mounted on the tractor are highlighted in Figure 12d. The accelerometers used for this experiment were KYOWA AS-1GBZ1 small-capacity acceleration transducers with rated capacities of $\pm 9.807 \text{ m/s}^2$ ($\pm 1 \text{ g}$). The frequency response given by the manufacturer is DC to 40 Hz at 23 °C. One sensor is mounted on the steel plate (labeled as vehicle body sensor), while another is mounted on a sprung wheel (labeled as vehicle axle sensor). These indirect measurements were used for scour detection. Vehicle velocities of $v_1 = 1.20 \text{ m/s}$ and $v_2 = 1.26 \text{ m/s}$ were used in these experiments. In order to examine experimental variability, the tested vehicles repeatedly passed over the bridge with these two velocities, and there were 30 times for each scenario. The scanning frequency in this laboratory experiment was 200 Hz.

In order to investigate the feasibility of the proposed approach, the drive-by concept that a traveling vehicle contains bridge information was first examined. For a bridge health condition, one run is randomly taken as an example. The indirect measurements of the two sensors are shown in Figure 13. Figure 14 plots the comparison of wavelet energies versus frequencies on these two signals. In this case, the speed of the vehicle is 1.20 m/s. As shown, the vehicle body acceleration presents peak energy close to the bounce frequency of the tractor (3.1 Hz), while the axle acceleration concentrates the energy at a frequency close to the bridge's first natural frequency. It is evident that it is difficult to extract the bridge information from the vehicle body acceleration when the test vehicle passes over the bridge. Those accelerations are not suitable for implementing indirect measurement. In contrast, vehicle axle acceleration shows clear bridge frequency information when the vehicle travels across the bridge. Therefore, only indirect measurements from the vehicle axle sensor were used for the study in the following. A frequency shift between the first

natural frequency of the bridge and the pseudo peak frequency of axle acceleration was also observed due to the driving frequency, as shown in Figure 3.

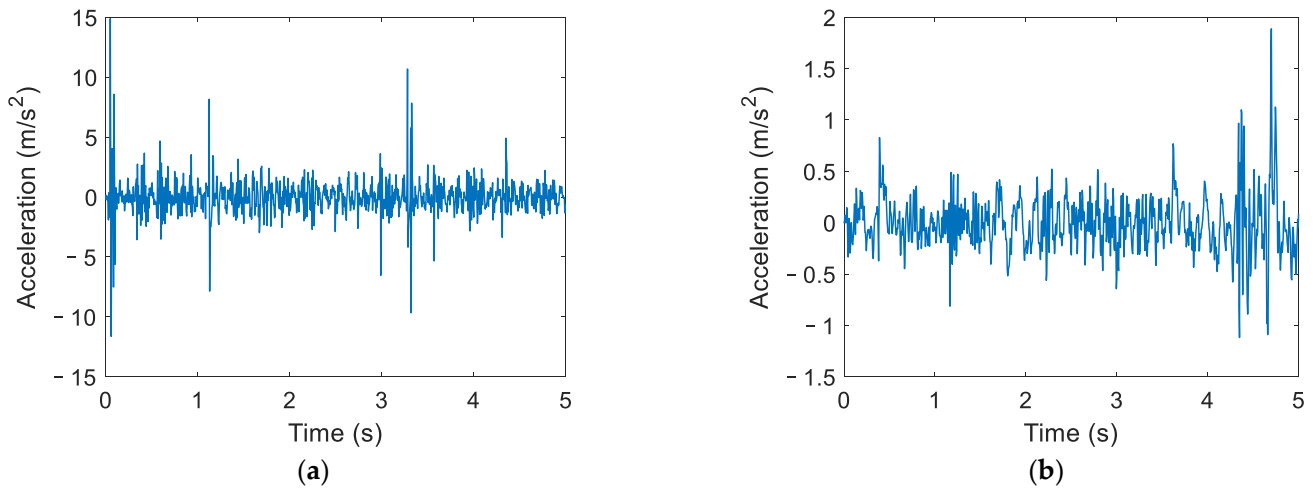


Figure 13. Indirect measurements: (a) acceleration of vehicle axle sensor; (b) acceleration of vehicle body sensor.

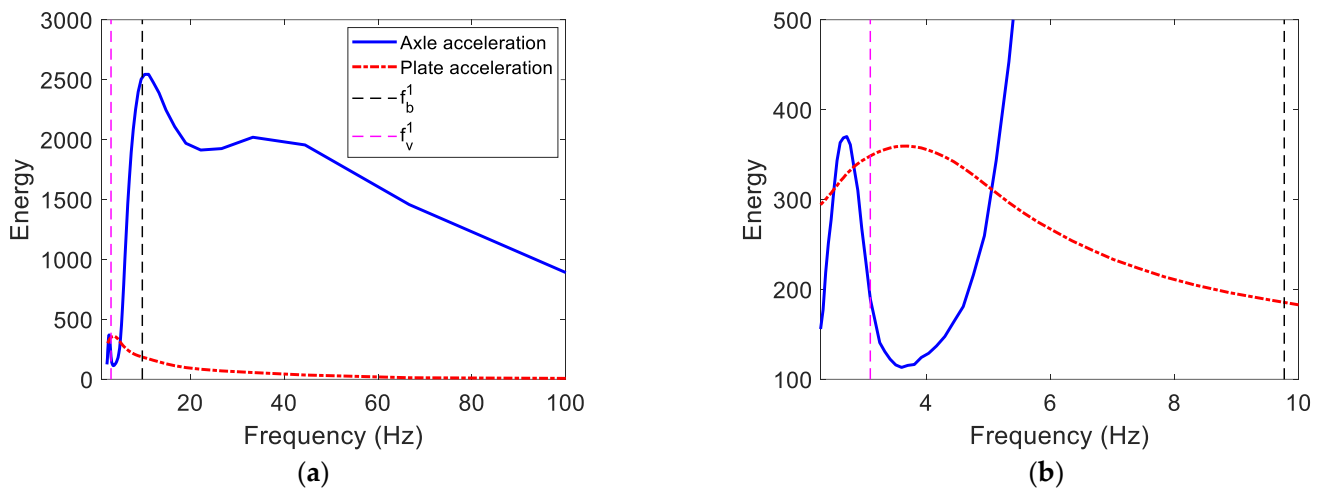


Figure 14. Wavelet energies vs. frequencies of two sensors: (a) frequency from 0 to 100 Hz; (b) frequency from 0 to 10 Hz (note: f_v^1 = the tractor bounce frequency).

For the vehicle speed of v_2 , there were 30 runs for each of the three bridge conditions on Pier 3, i.e., the health bridge, 24.5% scour damage, and 44.9% scour damage. Figure 15 shows the energy distributions for those three conditions with a boxplot. Similar to the simulation results, it is difficult to successfully detect the presence of scour using one or few runs due to the experimental variability. The proposed approach was then applied to this case. Three normal probability distributions were fitted on those runs under three bridge conditions. The mean values and ranges of $\mu \pm 0.5\sigma$ are plotted in Figure 16a. It was shown that the mean value of the normal probability distribution increases with the increase in scour damage level. In addition, the reference line (value of $\mu - 0.5\sigma$) for a higher scour level is greater than the baseline ($\mu + 0.5\sigma$) for a lower scour level, indicating that the presence of scour can be successfully detected using the proposed approach. In this case, the scour location indicators on piers were calculated and illustrated in Figure 16b. As expected, the scoured pier index of ID_{pier}^3 has the maximum value among $ID_{pier}^{1\sim3}$. It experimentally demonstrates that the proposed approach can effectively detect the presence of scour and identify the scour location.

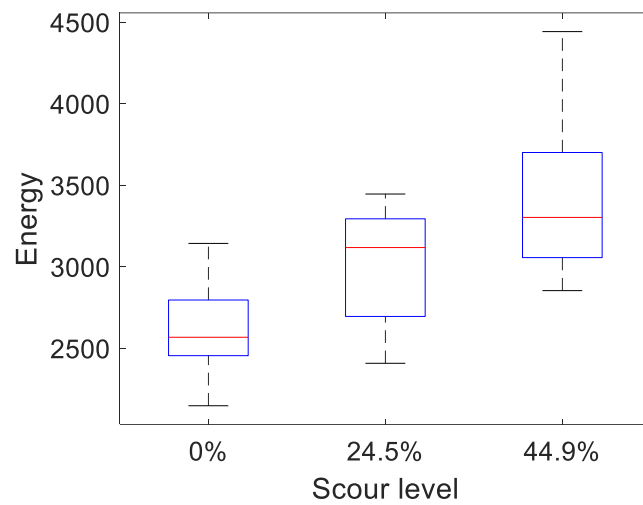


Figure 15. Boxplot of energy on different bridge conditions.

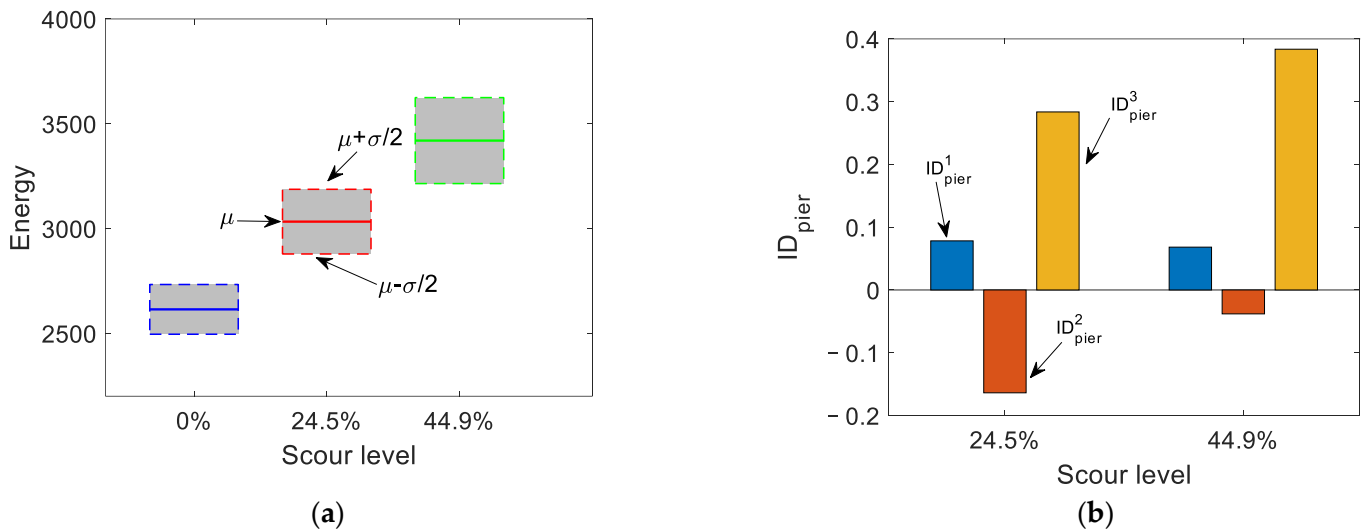


Figure 16. Results of scour detection on pier 3 with the speed of v_2 : (a) ranges of $\mu \pm 0.5\sigma$ for different bridge conditions; (b) scour location indicator on piers.

Similarly, the proposed approach was used to detect the scour on Pier 3 at the vehicle speed of v_1 . The results are illustrated in Figure 17. The mean values of distributions also clearly increase with the increase in scour damage level. However, in this case, the reference line (value of $\mu - 0.5\sigma$) of the scour damage level of 24.5% was not greater than the baseline (value of $\mu + 0.5\sigma$) for the health bridge. Therefore, the scour was not successfully detected using the proposed approach. The possible reason for this is the fewer runs for each scenario. There are only 30 runs for each scenario resulting in more uncertainty. It is believed that more runs can improve the identified result. Figure 17b shows the calculation of pier indexes. As shown, those pier indexes can still clearly reflect the scoured pier.

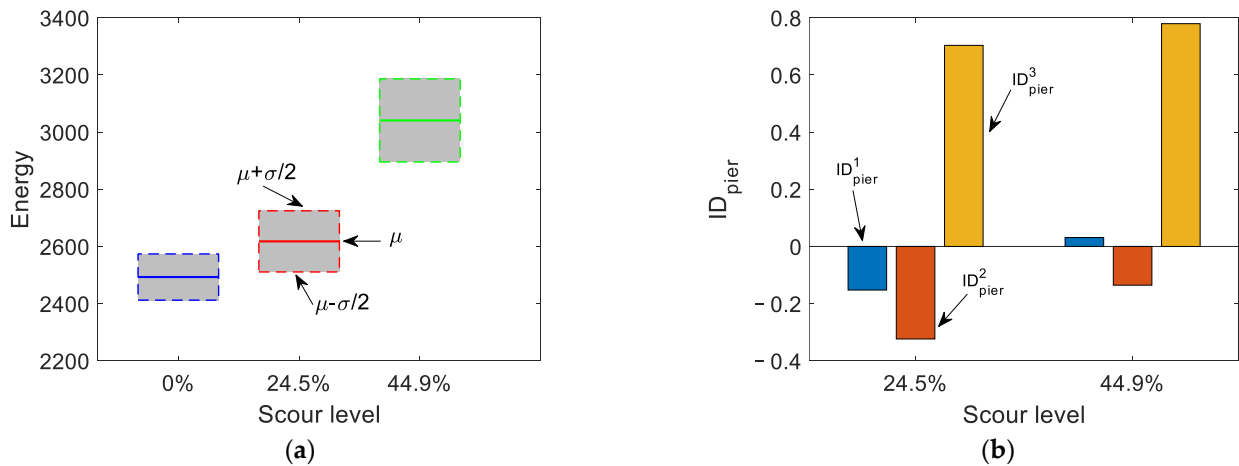


Figure 17. Results of scour detection on pier 3 with the speed of v_1 : (a) ranges of $\mu \pm 0.5\sigma$ for different bridge conditions; (b) scour location indicator on piers.

Figure 18 illustrates the scour detection results on Pier 2 at two speeds of v_1 and v_2 . Compared to the health bridge, the presence of scour can be successfully detected using the proposed approach for each case. However, for both velocities, it fails to reflect the change in wavelet energy from the scour damage level of 24.5% to the scour damage level of 44.9%. This is consistent with the phenomenon in the simulation. The change in wavelet energy is not sensitive to the high scour damage level on Pier 2. This change gradually decreases with the increase in the degree of scour damage. In addition, similar to the results in the simulation, it was found that for the lower scour level, the proposed approach is more sensitive to scour on Pier 2 than that on Pier 3. Figure 19 shows the results of detecting the scour location for two velocities. All results can successfully and clearly indicate the exact scoured pier.

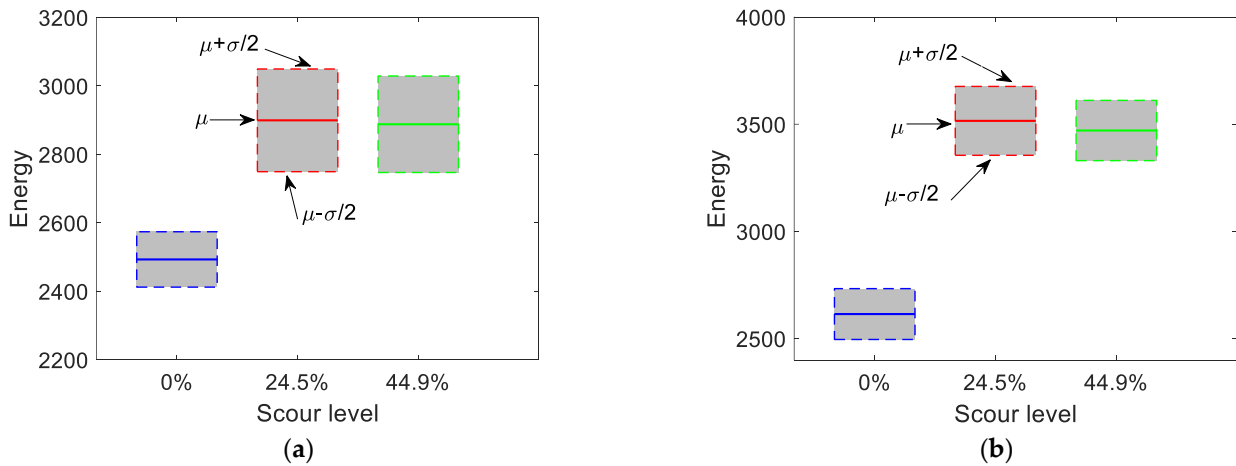


Figure 18. Ranges of $\mu \pm 0.5\sigma$ when scour occurs on Pier 2: (a) speed of v_1 ; (b) speed of v_2 .

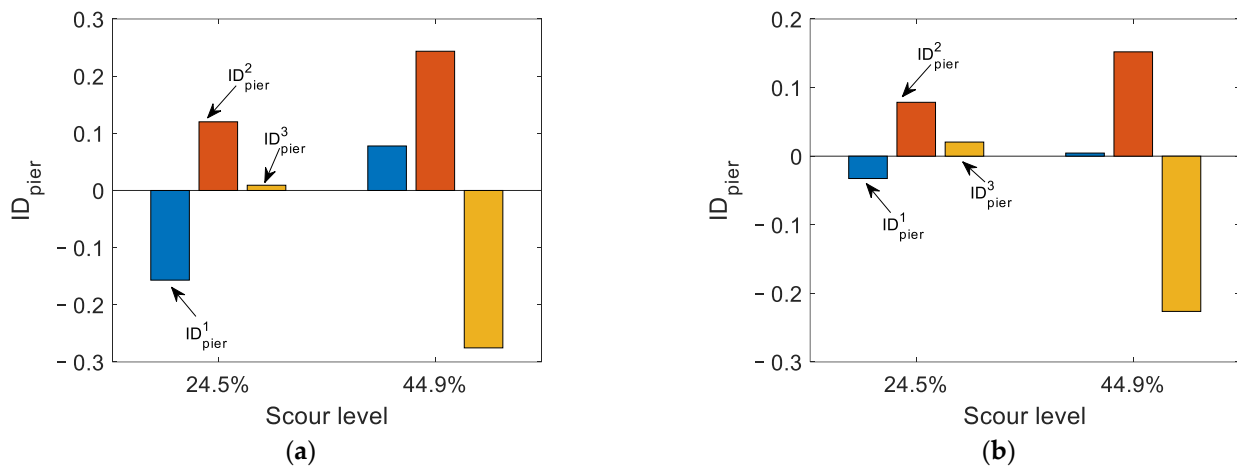


Figure 19. Scour location indicator on Pier 2: (a) speed of v_1 ; (b) speed of v_2 .

6. Conclusions

This paper proposed an approach to detect bridge scour and its location using indirect measurements from a passing vehicle. The feasibility of indirect measurement in scours detection was first verified by laboratory experiments in this study. The change in wavelet energy was used to reflect the loss in foundation stiffness resulting from bridge scour erosion. By considering the variability in the environment, a statistical-wavelet-based approach was then proposed. A normal probability distribution was used to fit a batch of test runs, and the distribution parameter (the mean value ± 0.5 times the standard deviation) was used to represent the bridge scour conditions. It concludes that the less batch of runs can detect scour faster but has a greater chance of making wrong decisions. It is suggested that the batch runs should not be less than 50. In addition, this paper proposed a pier index to identify the scoured pier. The effectiveness was validated by both simulation and experiment.

From the experimental test, it was found that the vehicle axle sensor is more sensitive to bridge information than that of the vehicle body sensor, which is more suitable for indirect bridge SHM. For the scour of Pier 3, the change in wavelet energy increases with the increasing degree of scour. While for the scour of Pier 2, this change gradually decreases with the increasing degree of scour. In other words, the proposed approach is not sensitive to the lower scour level on Pier 3, and it may be difficult to find the change in wavelet energy for the higher scour level on Pier 2.

Blind testing in numerical analysis simulates the entire process of on-site scour detection using the concept of “drive-by” SHM. The speed of the instrumented vehicle is as high as 14 m/s, which is an operational speed in practice. Compared to direct bridge SHM, the “drive-by” bridge SHM has no installation, maintenance, and power supply issues and has the advantages of low cost and convenience. The results in this paper will be of interest to the ongoing development of the scour monitoring field with indirect measurements. However, the development of scour detection using indirect measurements is relatively recent. Some issues are not addressed in this paper, e.g., multiple piers scour, variability in vehicle velocity, and field test demonstrations, which should be investigated in the ongoing work. In addition, there is only one type of vehicle used in this paper. Therefore, the proposed approach requires a specific instrumented vehicle for scour inspection. Mei [53] developed the concept of using vehicles of random traffic over the bridge for the drive-by bridge SHM. The smartphone inside the vehicles can be used as a sensor as well as an acquisition system. The bridge conditions can be monitored by random traffic, which significantly improves the efficiency of the proposed approach. Thus, further study on this will be investigated in the future.

Author Contributions: Conceptualization, B.Z. and C.T.; methodology, C.T.; software, C.T.; validation, B.Z.; formal analysis, B.Z.; investigation, B.Z. and C.T.; resources, E.J.O. and P.C.F.; data curation, C.-W.K.; writing—original draft preparation, B.Z. and C.T.; writing—review and editing, H.Z. and E.J.O.; visualization, H.Z.; supervision, H.Z.; project administration, H.Z.; funding acquisition, H.Z. and C.T. All authors have read and agreed to the published version of the manuscript.

Funding: This research was supported by the National Natural Science Foundation of China (52008162), the Key Research and Development Program of Hunan Province (2019SK2172), The Science and Technology Innovation Program of Hunan Province (2020RC2018), and Fellowship of China Postdoctoral Science Foundation (2020M680114).

Data Availability Statement: Not applicable.

Conflicts of Interest: The authors declare no conflict of interest.

References

1. Wardhana, K.; Hadipriono, F.C. Analysis of recent bridge failures in the United States. *J. Perform. Constr. Facil.* **2003**, *17*, 144–150. [[CrossRef](#)]
2. Briaud, J.-L.; Ting, F.; Chen, H.; Cao, Y.; Han, S.; Kwak, K. Erosion function apparatus for scour rate predictions. *J. Geotech. Geoenviron. Eng.* **2001**, *127*, 105–113. [[CrossRef](#)]
3. Malekjafarian, A.; Kim, C.-W.; O'Brien, E.J.; Prendergast, L.J.; Fitzgerald, P.C.; Nakajima, S. Experimental Demonstration of a Mode Shape-Based Scour-Monitoring Method for Multispan Bridges with Shallow Foundations. *J. Bridge Eng.* **2020**, *25*, 04020050. [[CrossRef](#)]
4. Malekjafarian, A.; Prendergast, L.J.; O'Brien, E. Use of mode shape ratios for pier scour monitoring in two-span integral bridges under changing environmental conditions. *Can. J. Civ. Eng.* **2020**, *47*, 962–973. [[CrossRef](#)]
5. Maddison, B. Scour failure of bridges. *Proc. Inst. Civ. Eng.-Forensic Eng.* **2012**, *165*, 39–52. [[CrossRef](#)]
6. Avent, R.R.; Alawady, M. Bridge scour and substructure deterioration: Case study. *J. Bridge Eng.* **2005**, *10*, 247–254. [[CrossRef](#)]
7. Brincker, R.; Zhang, L.; Andersen, P. Modal identification of output-only systems using frequency domain decomposition. *Smart Mater. Struct.* **2001**, *10*, 441. [[CrossRef](#)]
8. Foti, S.; Sabia, D. Influence of foundation scour on the dynamic response of an existing bridge. *J. Bridge Eng.* **2011**, *16*, 295–304. [[CrossRef](#)]
9. Prendergast, L.J.; Hester, D.; Gavin, K.; O'sullivan, J.J.; Vibration. An investigation of the changes in the natural frequency of a pile affected by scour. *J. Sound Vib.* **2013**, *332*, 6685–6702. [[CrossRef](#)]
10. Klinga, J.V.; Alipour, A. Assessment of structural integrity of bridges under extreme scour conditions. *Eng. Struct.* **2015**, *82*, 55–71. [[CrossRef](#)]
11. Prendergast, L.J.; Hester, D.; Gavin, K. Development of a vehicle-bridge-soil dynamic interaction model for scour damage modelling. *J. Shock Vib.* **2016**, *2016*, 7871089. [[CrossRef](#)]
12. Xiong, W.; Kong, B.; Tang, P.; Ye, J. Vibration-based identification for the presence of scouring of cable-stayed bridges. *J. Aerosp. Eng.* **2018**, *31*, 04018007. [[CrossRef](#)]
13. Kong, X.; Cai, C.-S.; Hu, J. The state-of-the-art on framework of vibration-based structural damage identification for decision making. *Appl. Sci.* **2017**, *7*, 497. [[CrossRef](#)]
14. Prendergast, L.J.; Gavin, K.; Hester, D. Isolating the location of scour-induced stiffness loss in bridges using local modal behaviour. *J. Civ. Struct. Health Monit.* **2017**, *7*, 483–503. [[CrossRef](#)]
15. Khan, M.A.; McCrum, D.P.; Prendergast, L.J.; O'Brien, E.J.; Fitzgerald, P.C.; Kim, C.-W. Laboratory investigation of a bridge scour monitoring method using decentralized modal analysis. *Struct. Health Monit.* **2021**, *20*, 3327–3341. [[CrossRef](#)]
16. Mosavi, A.A.; Seracino, R.; Rizkalla, S. Effect of temperature on daily modal variability of a steel-concrete composite bridge. *J. Bridge Eng.* **2012**, *17*, 979–983. [[CrossRef](#)]
17. Kim, J.-T.; Ryu, Y.-S.; Cho, H.-M.; Stubbs, N. Damage identification in beam-type structures: Frequency-based method vs. mode-shape-based method. *Eng. Struct.* **2003**, *25*, 57–67. [[CrossRef](#)]
18. Carden, E.P.; Fanning, P. Vibration based condition monitoring: A review. *Struct. Health Monit.* **2004**, *3*, 355–377. [[CrossRef](#)]
19. Scozzese, F.; Ragni, L.; Tubaldi, E.; Gara, F. Modal properties variation and collapse assessment of masonry arch bridges under scour action. *Eng. Struct.* **2019**, *199*, 109665. [[CrossRef](#)]
20. Fan, W.; Qiao, P. Vibration-based damage identification methods: A review and comparative study. *Struct. Health Monit.* **2011**, *10*, 83–111. [[CrossRef](#)]
21. Döhler, M.; Lam, X.-B.; Mevel, L. Uncertainty quantification for modal parameters from stochastic subspace identification on multi-setup measurements. *Mech. Syst. Signal Process.* **2013**, *36*, 562–581. [[CrossRef](#)]
22. Sim, S.-H.; Spencer Jr, B.; Zhang, M.; Xie, H.J.S.C.; Monitoring, H. Automated decentralized modal analysis using smart sensors. *Struct. Control Health Monit.* **2010**, *17*, 872–894. [[CrossRef](#)]
23. Tan, C.; Elhattab, A.; Uddin, N. Wavelet-Entropy Approach for Detection of Bridge Damages Using Direct and Indirect Bridge Records. *J. Infrastruct. Syst.* **2020**, *26*, 04020037. [[CrossRef](#)]

24. Yang, Y.B.; Lin, C.W.; Yau, J.D. Extracting bridge frequencies from the dynamic response of a passing vehicle. *J. Sound Vib.* **2004**, *272*, 471–493. [[CrossRef](#)]
25. Yang, Y.B.; Yang, J.P. State-of-the-Art Review on Modal Identification and Damage Detection of Bridges by Moving Test Vehicles. *Int. J. Struct. Stab. Dyn.* **2018**, *18*, 1850025. [[CrossRef](#)]
26. Kong, X.; Cai, C. Scour effect on bridge and vehicle responses under bridge–vehicle–wave interaction. *J. Bridge Eng.* **2016**, *21*, 04015083. [[CrossRef](#)]
27. Fitzgerald, P.C.; Malekjafarian, A.; Cantero, D.; OBrien, E.J.; Prendergast, L.J. Drive-by scour monitoring of railway bridges using a wavelet-based approach. *Eng. Struct.* **2019**, *191*, 1–11. [[CrossRef](#)]
28. Zhu, X.Q.; Law, S.S. Wavelet-based crack identification of bridge beam from operational deflection time history. *Int. J. Solids Struct.* **2006**, *43*, 2299–2317. [[CrossRef](#)]
29. Shahsavari, V.; Chouinard, L.; Bastien, J. Wavelet-based analysis of mode shapes for statistical detection and localization of damage in beams using likelihood ratio test. *Eng. Struct.* **2017**, *132*, 494–507. [[CrossRef](#)]
30. Rucka, M.; Wilde, K. Application of continuous wavelet transform in vibration based damage detection method for beams and plates. *J. Sound Vib.* **2006**, *297*, 536–550. [[CrossRef](#)]
31. Hou, Z.; Noori, M.; St Amand, R. Wavelet-based approach for structural damage detection. *J. Eng. Mech.* **2000**, *126*, 677–683. [[CrossRef](#)]
32. Cantero, D.; Basu, B. Railway infrastructure damage detection using wavelet transformed acceleration response of traversing vehicle. *Struct. Control Health Monit.* **2015**, *22*, 62–70. [[CrossRef](#)]
33. Chatterjee, P.; OBrien, E.; Li, Y.Y.; Gonzalez, A. Wavelet domain analysis for identification of vehicle axles from bridge measurements. *Comput. Struct.* **2006**, *84*, 1792–1801. [[CrossRef](#)]
34. Hester, D.; Gonzalez, A. A wavelet-based damage detection algorithm based on bridge acceleration response to a vehicle. *Mech. Syst. Signal Process.* **2012**, *28*, 145–166. [[CrossRef](#)]
35. OBrien, E.J.; McCrum, D.P.; Khan, M.A.; Prendergast, L.J. Wavelet-based operating deflection shapes for locating scour-related stiffness losses in multi-span bridges. *Struct. Infrastruct. Eng.* **2021**. [[CrossRef](#)]
36. Fitzgerald, P.C.; Malekjafarian, A.; Bhowmik, B.; Prendergast, L.J.; Cahill, P.; Kim, C.W.; Hazra, B.; Pakrashi, V.; OBrien, E.J. Scour Damage Detection and Structural Health Monitoring of a Laboratory-Scaled Bridge Using a Vibration Energy Harvesting Device. *Sensors* **2019**, *19*, 2572. [[CrossRef](#)] [[PubMed](#)]
37. Cebon, D. *Handbook of Vehicle-Road Interaction*; Swets & Zeitlinger: Lisse, The Netherlands, 1999.
38. Tan, C.; Elhattab, A.; Uddin, N. “Drive-by” bridge frequency-based monitoring utilizing wavelet transform. *J. Civ. Struct. Health Monit.* **2017**, *7*, 615–625. [[CrossRef](#)]
39. Federal Emergency Management Agency (FEMA). *Prestandard and Commentary for the Seismic Rehabilitation of Buildings*; FEMA 356: Washington, DC, USA, 2000.
40. Pais, A.; Kausel, E. Approximate formulas for dynamic stiffnesses of rigid foundations. *Soil Dyn. Earthq. Eng.* **1988**, *7*, 213–227. [[CrossRef](#)]
41. Mylonakis, G.; Nikolaou, S.; Gazetas, G. Footings under seismic loading: Analysis and design issues with emphasis on bridge foundations. *Soil Dyn. Earthq. Eng.* **2006**, *26*, 824–853. [[CrossRef](#)]
42. ISO. *Mechanical Vibration—Road Surface Profiles—Reporting of Measured Data*; International Organization for Standardization: Geneva, Switzerland, 1995.
43. Yang, Y.B.; Yau, J.; Yao, Z.; Wu, Y. *Vehicle-Bridge Interaction Dynamics: With Applications to High-Speed Railways*; World Scientific: Singapore, 2004.
44. Gao, R.X.; Yan, R. *Selection of Base Wavelet*, 1st ed.; Springer: Boston, MA, USA, 2011; pp. 165–187.
45. Zhao, H.; Tan, C.; OBrien, E.J.; Uddin, N.; Zhang, B. Wavelet-Based Optimum Identification of Vehicle Axles Using Bridge Measurements. *Appl. Sci.* **2020**, *10*, 7485. [[CrossRef](#)]
46. Cantero, D.; McGetrick, P.; Kim, C.W.; OBrien, E. Experimental monitoring of bridge frequency evolution during the passage of vehicles with different suspension properties. *Eng. Struct.* **2019**, *187*, 209–219. [[CrossRef](#)]
47. Malekjafarian, A.; Brien, E.J. Identification of bridge mode shapes using Short Time Frequency Domain Decomposition of the responses measured in a passing vehicle. *Eng. Struct.* **2014**, *81*, 386–397. [[CrossRef](#)]
48. OBrien, E.J.; Fitzgerald, P.C.; Malekjafarian, A.; Sevillano, E. Bridge damage detection using vehicle axle-force information. *Eng. Struct.* **2017**, *153*, 71–80. [[CrossRef](#)]
49. Prendergast, L.; Reale, C.; Gavin, K. Probabilistic examination of the change in eigenfrequencies of an offshore wind turbine under progressive scour incorporating soil spatial variability. *Mar. Struct.* **2018**, *57*, 87–104. [[CrossRef](#)]
50. Williams, E.J.; Drexler, J.S. A non-destructive method for determining peanut pod maturity. *Peanut Sci.* **1981**, *8*, 134–141. [[CrossRef](#)]
51. Simola, K.; Pulkkinen, U.J.R.E.; Safety, S. Models for non-destructive inspection data. *Reliab. Eng. Syst. Saf.* **1998**, *60*, 1–12. [[CrossRef](#)]
52. Adhikary, S.; Singh, Y.; Paul, D. Modelling of soil-foundation-structure system. *Soil Dyn. Earthq. Eng.* **2014**, *61*, 13–28. [[CrossRef](#)]
53. Mei, Q.; Gül, M.; Boay, M.J.M.S.; Processing, S. Indirect health monitoring of bridges using Mel-frequency cepstral coefficients and principal component analysis. *Mech. Syst. Signal Process.* **2019**, *119*, 523–546. [[CrossRef](#)]